crystals

MDPI

Article

Novel Functional Materials of Hydrogen Storage $B_{20}N_{24}$: A First-Principles Calculation

Jing Zhao [1], Zhongtang Huo [2], Shuailei Xu [1], Mei Xiong [3,*], Dezheng Liu [1], Yikun Wang [1] and Xin Jia [4]

[1] Hubei Longzhong Laboratory, School of Mechanical Engineering, Hubei University of Arts and Science, Xiangyang 441053, China; zhaojing@hbuas.edu.cn (J.Z.)
[2] Mechanical and Electrical College, Handan University, Handan 056001, China
[3] Tianjin Key Laboratory of High Speed Cutting and Precision Machining, Tianjin University of Technology and Education, Tianjin 300222, China
[4] State Key Laboratory of Metastable Materials Science and Technology, Yanshan University, Qinhuangdao 066004, China; jx30307787@163.com
* Correspondence: xiongmei_1327@163.com

Abstract: In this paper, a N-rich B–N polymorph named as $B_{20}N_{24}$ is proposed through first-principles calculations. The stability of the $B_{20}N_{24}$ polymorph at ambient conditions is confirmed using the phonon dispersion spectra and the Born stability criteria. Electronic properties calculations show that $B_{20}N_{24}$ exhibits a semiconducting feature, with a 0.87 eV direct band gap derived from HSE06 functions, which is much lower than many other B–N polymorphs. Specifically, owing to its cage-like framework, $B_{20}N_{24}$ may be used in hydrogen storage at a capacity of ~6.8 wt.%. The $B_{20}N_{24}$ polymorph enriches the B–N system theoretically, and this polymorph is promising for use in electronic devices and hydrogen storage.

Keywords: first-principles calculations; B–N compounds; N-rich B–N polymorphs; functional materials; hydrogen storage

check for updates

Citation: Zhao, J.; Huo, Z.; Xu, S.; Xiong, M.; Liu, D.; Wang, Y.; Jia, X. Novel Functional Materials of Hydrogen Storage $B_{20}N_{24}$: A First-Principles Calculation. *Crystals* **2023**, *13*, 1029. https://doi.org/10.3390/cryst13071029

Academic Editor: Bo Chen

Received: 27 April 2023
Revised: 10 June 2023
Accepted: 22 June 2023
Published: 28 June 2023

1. Introduction

Boron nitride (BN) compounds have attracted much interest because of their intriguing behaviors. As for the experimental aspect, given that novel BN polymorphs with unique properties are synthesized, the potential applications of BN polymorphs in electronic devices and industries have increased. For example, the successfully synthesized nano-twinned cBN enhances the physical properties of cBN [1], such as a hardness value exceeding 100 GPa and an oxidization temperature achieving 1294 °C. Additionally, novel BN polymorphs with various morphological features, such as BN cluster [2], BN nanotube [3], BN nanosheets and nano-meshes [4,5], have been synthesized successfully, thereby enriching the applications of BN materials. Moreover, the ultralight three-dimensional (3D) BN foam [6], which has high permittivity and thermal stability, is a new ultralight material that can be used in water cleaning.

Some BN polymorphs synthesized in experiments have a B/N ratio of about 1.0, and this phenomenon is predominantly caused by defects in materials [7–9]. Theoretical studies have shown that many BN clusters with different sizes, such as $B_{12}N_{12}$ and $B_{36}N_{36}$ fullerene-like cluster, can be constructed [10–12]. Previous studies showed that the stoichiometric BN compound with purely B–N bonds in crystal structures is the generally stable framework and that nonstoichiometric frameworks may lead to energetic, unfavorable B–B and N–N dimers. However, nonstoichiometric BN structures have also been constructed in previous studies. Simone et al. [13] reported the first-principles calculations of the role of stoichiometry in the structure and energy of BN clusters. Results showed that $B_{32}N_{36}$ and $B_{60}N_{64}$ are more stable than their stoichiometric counterparts in a N-rich environment, even when dimers exist in the framework. Simultaneously, B–B and N–N bonds are unavoidable

in these B-rich or N-rich BN polymorphs, and the reality is unclear as to the stability of N-rich B–N compounds which are constructed with purely B–N bonds.

Recently, many novel BN allotropes have been proposed [14,15], given the electronegative difference between the two elements. Wang et al. [14] reported a novel phase of boron nitride m-BN, in which, when utilizing the GGA (generalized gradient approximation) and LDA (local density approximation) functionals, the lattice constant of c-BN with the GGA functional is 0.166% higher than that of the experimental value, while the results of the LDA functional are 1.409% smaller than that of the experimental value. The results indicated that the m-BN is mechanically stable and dynamically stable, which makes for an indirect and wide band-gap semiconductor material, and the Fermi level and the band gap are not sensitive to the effect of pressure. In addition, m-BN is a potential superhard material with a hardness of 56.1 GPa. Most of the polymorphs composited with B and N have a stoichiometric B:N ratio of 1:1 [16–24]. For example, the tetragonal bct-BN [25], orthorhombic phase Z-BN [16], and P-BN [20], have been predicted, and both of them are constructed with 4- and 8-atom rings per unit cell. In terms of electronic properties, all BN allotropes mentioned above are semiconductors. Recently, several 3D metallic BN allotropes have been predicted by Dai et al. [18], Zhang et al. [21], etc. These metallic BN allotropes, which are different from conventional BN ceramics, can lead to new applications in electronic devices. In considering several N-rich B–N polymorphs, [26–28]. Li et al. [26] discovered that $C222_1$-B_3N_5 was a metastable material that can be recovered under ambient conditions, making it a promising high-energy-density material with an energy density of 3.44 kJ/g. Additionally, stress–strain calculations estimated a Vicker's hardness of approximately 44 GPa. Structure searching also revealed a new sodalite-like clathrate BN structure that was metastable under ambient conditions. He et al. [27] reported that t-B_3N_4, with structural units composed of sp^3 c-BN blocks and sp^2 N–N bonds, is metastable at ambient pressure but becomes energetically more stable than layered B_3N_4, h-BN, or N_2 under pressure. The electronic structure analysis showed that t-B_3N_4 was planar conductive with conduction interrupted by insulated B atomic layers along the c-axis. This unique 2D metallicity in 3D t-B_3N_4 has potential applications in electronic devices. The calculated Vickers hardness of t-B_3N_4 exceeded 40 GPa, indicating its superhard nature. Moreover, due to the strong N–N bonds along the c-axis, the axial ultra-incompressibility of t-B_3N_4 was even greater than that of c-BN and diamond. This type of boron nitride exhibited the combined electrical and mechanical properties of 2D metallicity in a 3D framework, in addition to superhardness and ultra-incompressibility. These findings open a new view of B–N functional materials.

In recent years, N-rich B–N polymorphs, such as superhard phases ($C222_1$-B_3N_5, B_2N_3) and metallic t-B_3N_4, have been predicted as novel functional materials, behaving as potential high-energy-density materials, due to the high energy of N–N dimers in their framework. In this work, $B_{20}N_{24}$ is constructed with fully B–N bonds, indicating that it is not a potential high-energy-density material. Moreover, hydrogen as a renewable energy has drawn people's attention for many years, but one limited problem in its widespread application is the storage medium. In terms of advantages in gravimetric density, light element compounds, such as carbon materials, including C_{60} fullerene and carbon nanotube, are good candidates for hydrogen storage. In recent years, extensive studies showed that porous BN polymorphs and BN cages exhibit promising applications in hydrogen storage [29,30]. For example, studies showed that BN nanotubes can store hydrogen at as much as 2.6 wt.% [29], and the $B_{36}N_{36}$ cage can reach to 4 wt.% [30]. Considering the cage-like structural features and low density of $B_{20}N_{24}$, it might be a candidate for hydrogen storage.

As previous studies have shown, structural prediction of a system can be executed via various methods, such as structural search programs, simulated annealing [10,11], basin hopping [14,15], metadynamics [16,17], evolutionary metadynamics [18,19], and so on. Additionally, given the structural similarities among different systems, more and more novel structures are predicted by changing the atoms of the revealed structures

which have been synthesized or proposed in some other system or study. Carbon and BN are isoelectronic in structure, with many phases of the two systems sharing the same configurations. Some examples include: diamond and cubic BN, hexagonal diamond and wurtzite BN, carbon nanotube and BN nanotube, graphene and BN nanoribbons, and so on. Moreover, the Cco-C8 structure of carbon allotrope has been predicted to be a candidate for cold-compressed graphite. Crystals sharing the same framework within different systems not only exist in carbon and BN compounds, but also can be found in some other classes. Several crystal structures, such as rock-salt-type BN, have been proposed as a high-pressure phase of a BN compound, one which shares the framework of rock-salt crystal [31,32]. Therefore, z-BN with the same framework as Cco-C8 is proposed as a novel phase for a BN compound. It is therefore viable to change a carbon structure into B and N atoms alternatively during the BN structure-prediction process.

In this paper, considering the structural similarities between carbon and BN allotropes, the structure-searching processes are carried out in two steps. Firstly, carbon structure research processing is conducted. Secondly, we selected some carbon structures with cage-like configurations, replacing C atoms with B and N atoms alternatively, in order to avoid the B–B and N–N dimers in the framework. As a result, a three-dimensional cage-like $B_{20}N_{24}$ polymorph as a candidate for hydrogen storage is predicted.

2. Calculation Methods

We implemented the structural searching of carbon allotropes at ambient conditions through the CALYPSO code [33]. This method can predict novel structures, and facilitates the composition of known chemical compounds. The underlying structural relaxation was performed using the density functional theory within the local density approximation (LDA) as implemented in the Vienna Ab Initio Simulation Package (VASP) [34]. Subsequent structural optimizations and properties calculations were performed using ultrasoft pseudopotentials with a plane wave cutoff energy of 280 eV in the Cambridge Serial Total Energy Package (CASTEP) [35]. The electron–electron exchange interaction was described using the exchange-correlation function of Ceperley and Alder [36], as parametrized by Perdew and Zunger (CA-PZ) [37] in the LDA. To obtain a more accurate determination of electronic properties, band structure calculations were conducted using the hybrid Heyd–Scuseria–Ernzerhof function (HSE06) [38]. The k-point spacing of $2\pi \times 0.04$ Å was generated by the k-point grid within the Monkhorst–Pack scheme [39]. The elastic properties are predicted with CASTEP code. In this process, a unit cell was adopted. The elastic constants C_{ij} were derived based on the strain–stress relationship (Hooke's law), which is within the range of elastic deformation; a finite strain was applied to the optimized structure, and the applied strain and the resulting stress were obtained [30]. The maximum applied strain amplitude was 0.3%, and the number of steps for each strain was set to 9 for this calculation. To verify the accuracy of our calculations, we calculated the lattice parameters and bond length for diamond and cubic BN. The results show that the lattice parameters of diamond and cubic BN are a = 3.528 Å and a = 3.580 Å, and the bond lengths of the C–C and B–N bonds are 1.528 Å and 1.550 Å, respectively, which are close to the results derived from experiments (3.567 Å and 1.545 Å for diamond, 3.615 Å and 1.565 Å for cubic BN). Therefore, we supposed that the calculations in this paper are feasible.

3. Results and Discussion

After structure-searching progresses, several carbon allotropes, such as diamond, graphite and CCo-C_8 [40] were obtained. These results confirmed the feasibility of our structural search methodology. Firstly, carbon allotropes with 8~30 atoms in per unit cell were systematically explored based on the first-principles calculations. Secondly, according to the geometries of carbon structures, we have selected some of the special configurations. During this process, these structures with odd rings are thrown away to avoid forming high energy B–B/N–N bonds in the atom's process of subsequent change. Therefore, some cage-like carbon structures composed of even-membered rings are retained. Finally, carbon

atoms are replaced with B and N atoms alternatively to avoid B–B/N–N bonds in the search for stable nonstoichiometric B–N polymorphs. Notably, according to the low energy and structure features, six cubic carbon allotropes, which had 7, 28, 44, 52, and 60 atoms in per unit cell, respectively, are selected among thousands of obtained novel carbon structures. The structural and geometric properties of these selected allotropes are investigated. The results show a mechanical and dynamical stable structure among these obtained structures, which is named as $B_{20}N_{24}$.

Figure 1 shows the optimized novel crystal structure and structural features of $B_{20}N_{24}$. At ambient pressure, three nonequivalent atoms assemble in a cubic lattice (space group *I-43m*) with a = b = c = 7.01 Å lattice parameter (Figure 1a). The Wyckoff atom positions of two nonequivalent B atoms, B1 and B2, are occupied 2d (0, 1/2, 1/4), 8c (0.3, 0.7, 0.3), and one N1 atom is occupied 24g (0.126, 0.625, 0.874), respectively. Figure 1a shows the primitive cell of the $B_{20}N_{24}$ polymorph. B1-N1-B2 atoms composed the hexagonal rings which can be viewed as puckered hBN layers, and these layers are connected to form a three-dimensional (3D) periodicity structure via sp^3-hybrid B2 atoms. As shown in Figure 1b, the unit cell of the $B_{20}N_{24}$ polymorph can be viewed as a cage-like structure, one which the hBN-liked layers connected with B–N single bonds to form a cage with an open boundary. The opened cage-like structure connects with the gap's overlapping and forms a 3D cage-like network with different cage-size in it (Figure 1c). The B1 atom at the 8*c* site is a trigonal coordinate with a trigonal N atom added to form B–N bond with length of d_1 = 1.43 Å, which is close to that of the sp^2-hybrid B–N bonds in hBN. The B2 atom at the 12*d* site is a tetragonal coordinate with a trigonal N atom with a B–N distance of d_1 = 1.52 Å; when the two combine cages together and construct the 3D N-rich BN allotropes, it is comparable to the sp^3-hybrid B–N bonds in cBN structure.

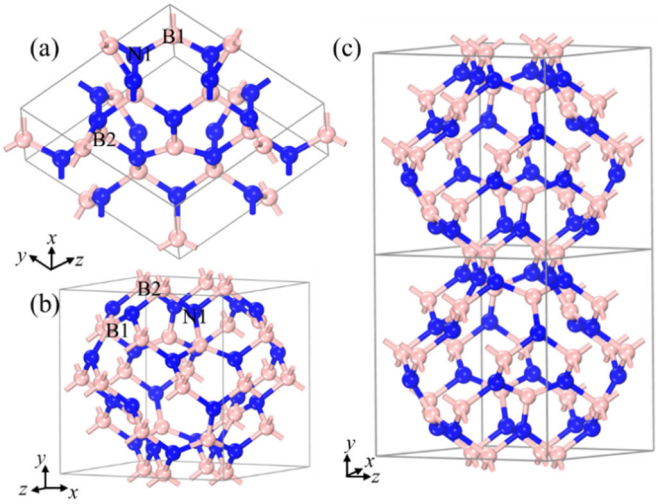

Figure 1. Structural configurations of $B_{20}N_{24}$: (**a**) primitive cell, (**b**,**c**) unit cell. The pink and blue balls stand for B and N atoms, respectively.

In order to clarify the energetic stability of the $B_{20}N_{24}$ polymorph, we calculated the formation energy via alpha-B and alpha-N_2 as precursors; the results of the convex hull of B–N compounds are plotted in Figure 2. As shown in Figure 2, the formation energies of some other B–N polymorphs are determined per-atom for comparison. As previous studies show, the layer-like h-B_3N_5 and h-B_2N_3 structures are stable at ambient pressure, and the bulked C_{2221}-B_3N_5 [26] and t-B_2N_3 [28] are metastable, which can derive from the stable phase under high pressure conditions. Additionally, the bulked t-B_3N_4 [27] is at a metastable phase at ambient pressure. One can see that the formation energy of $B_{20}N_{24}$ is beyond the line at the N-rich part, so we have supposed that the $B_{20}N_{24}$ polymorph is at a metastable phase at ambient pressure.

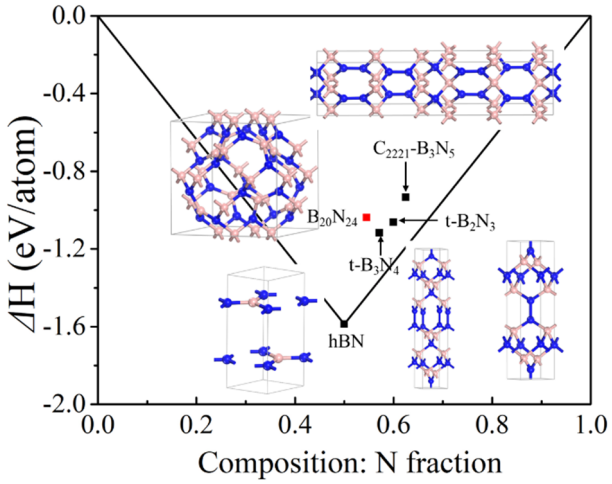

Figure 2. Convex hull diagram for the B−N compound at ambient pressure. The formation energies are defined as ΔH = [1/(x + y)]H(BxNy) − [xH(B) +yH(N)]), in which the alpha-B phase and alpha-N_2 structures are used in the formula, respectively.

The mechanical stability of $B_{20}N_{24}$ is validated by elastic constants calculations. The calculated elastic constants are C_{11} = 427.0 GPa, C_{44} = 240.4 GPa, and C_{12} = 184.2 GPa, respectively. The structure of $B_{20}N_{24}$ possesses cubic lattice and the known Boron stability criteria for cubic lattice [41], i.e., $C_{11} > 0$, $C_{44} > 0$, $C_{11} > |C_{12}|$, $(C_{11} + 2C_{12}) > 0$. Obviously, these elastic constants satisfy the Boron stability criteria, thereby confirming that $B_{20}N_{24}$ is mechanically stable. Phonon dispersion curves were used to confirm the dynamic stability of $B_{20}N_{24}$, which is characterized by a lack of imaginary frequencies across the whole spectrum; the results are plotted in Figure 3. No imaginary frequency is observed across the whole Brillion Zone, indicating that $B_{20}N_{24}$ is dynamically stable. Therefore, we suppose that the $B_{20}N_{24}$ polymorph is at a metastable phase at ambient conditions.

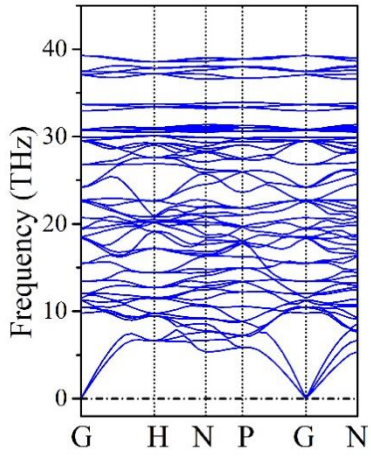

Figure 3. Phonon dispersion spectrum of $B_{20}N_{24}$.

The electronic properties of $B_{20}N_{24}$ are studied by calculating the band structures and corresponding partial density of state (PDOS); the results are plotted in Figure 4. As shown in Figure 4a, the $B_{20}N_{24}$ structure exhibits a 0.87 eV direct band gap. In order to study the origination of valance band minima (VBM) and conductive band maximum (CBM), we further calculated the PDOS of three nonequivalent atoms PDOS in the framework, and the results are shown in Figure 4b–e. In Figure 4b, the electronic states at the Fermi level originate from the 2*p* orbits, and Figure 4c–e shows that the CBM and most of the VBM of $B_{20}N_{24}$ are contributed from the 2*p* state of N1 atoms. The contributions of B1 and B2 atoms to the CBM and VBM can be neglected.

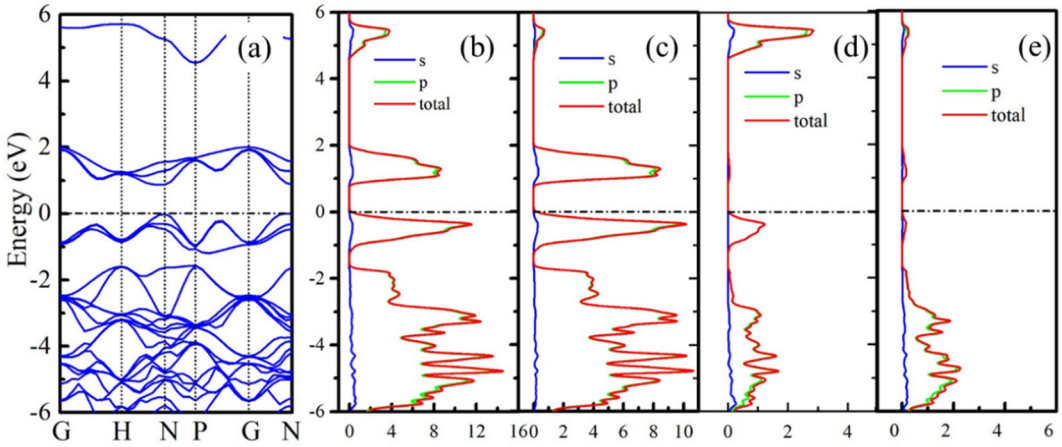

Figure 4. Electronic properties of $B_{20}N_{24}$ structure: (**a**) band structure, (**b**) PDOS, and (**c**–**e**) PDOS of N1, B1, and B2 atoms, respectively. The dotted lines reprents Femi level.

In the following section, the endohedral H_2 molecule storage in $B_{20}N_{24}$ has been studied systematically. For a single H_2 molecule, we set it as occupying the center of the $B_{20}N_{24}$ cage and ignore other simultaneous sites. In other conditions, ones with more than one H_2 molecule, H_2 molecules are laid into the $B_{20}N_{24}$ cage randomly and kept isolated from each other, keeping the distance between two H_2 molecules larger than 0.74 Å (the H–H bond length in a H_2 molecule). The calculated formation energies with different n values are plotted in Figure 5. The formation energy of the $n$$H_2$@$B_{20}N_{24}$ complex is defined as: $E_f = E_{(BN+nH2)} - E_{BN} - nE_{H2}$, where $E_{(BN+nH2)}$ is the total energy of $n$$H_2$@$B_{20}N_{24}$ complex, E_{BN} and E_{H2} are the total energy of $B_{20}N_{24}$ and H_2 molecules, respectively, and n stands for the number of H_2 molecules set in the $B_{20}N_{24}$ polymorph. Figure 6 shows the atomic configurations of the $n$$H_2$@$B_{20}N_{24}$ complex. At n = 1, the H_2 molecule is set at the center of the framework (Figure 6a). Figure 6b shows the H_2@$B_{20}N_{24}$ complex after full geometrical optimization; the formation energy is −0.28 eV/atom. The H_2 molecule is isolated in the $B_{20}N_{24}$ cage, B-H and N-H bonds are not presented in this complex, and the H_2 molecule has a stretched H-H bond length of 0.777 Å. The volume of the complex (348.8 Å^3) is larger than that of $B_{20}N_{24}$ (347.5 Å^3), which means that the H_2 molecule brings out a structural deformation. As we know, a negative formation energy means an exothermic reaction and energetic-favorable status, indicating that the $n$$H_2$@$B_{20}N_{24}$ complex is stable relative to decomposition into a B–N compound and H_2 molecules. Therefore, we supposed that it was possible to form H_2@$B_{20}N_{24}$ complex at ambient conditions with a suitable precursor and method. As H_2 molecules increase, the distance between H_2 molecules becomes shorter and shorter, resulting in repulsive interactions between H_2 molecules; the attractive interactions between H_2 molecules and B/N atoms increase correspondingly. This induced a change in the bonding conditions of the complex after the full relaxation of the complex.

During the geometric optimization process, the H_2 molecules in the $B_{20}N_{24}$ cage move away from their initial position where we have set them initially, leading to some of the H_2 molecules remaining molecular and some others not. Giving the dangling bonds in the configuration, some H_2 molecules dissociate to bind with N/B atoms and form N-H/B-H bonds (Figure 6c). Interestingly, during this process, H atoms bind with N atoms more than with B atoms; this might be caused by fact that the N atom has higher electronegativity difference than does the B atom. The sp^3 rehybridization of the formation of N-H/B-H bonds minimizes the total energy of the complex, and as the number of H_2 molecules increases, the number of dissociated H_2 molecules is decreased. Thus, the formation energy decreases from n = 1 to n = 10, and has a minimum value at n = 10, illustrating that the 10H_2@$B_{20}N_{24}$ complex is the most stable state of the $n$$H_2$@$B_{20}N_{24}$ complex. After that, as the H_2 molecule increases, at n = 11–16, the total energy of complex increases and tends to become positive. We supposed that this is because, with the increase of the number of

hydrogen molecules in this BN structure, the framework of $nH_2@B_{20}N_{24}$ complex acquires more and more deformation. In this, B–N bonds are expanded, thereby inducing the high energy of B–N chemical bonds; also, the repulsion between H atoms is increased as the distance of H atoms grows closer, in order to attain the equilibrium state for the complex. Therefore, the energy levels of the $nH_2@B_{20}N_{24}$ complexes are raised. For $nH_2@B_{20}N_{24}$ complexes with n = 17, 18, and 19, the formation energies are positive, indicating that the storage is an endoergic reaction. When n = 20, several B–N bonds, such as the bond between the B–N pair (marked with red circles in Figure 6d), are stretched to ~1.75 Å, showing that B–N bonds are destroyed, while the H_2 molecules remain in the cage. However, the number of n increases to 21, and the framework of the $nH_2@B_{20}N_{24}$ complex is broken, resulting in a number of escaped H_2 molecules. Therefore, the maximum H_2 molecule storage capacity of $H_2@B_{20}N_{24}$ is 19, which corresponds to a gravimetric proportion of 6.8 wt.%.

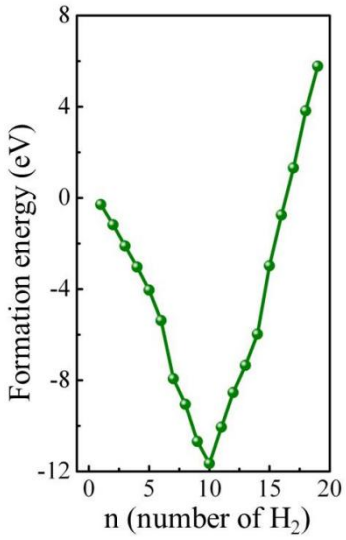

Figure 5. Formation energies of the $nH_2@$ $B_{20}N_{24}$ complex as a function of the number of H_2 molecules stored.

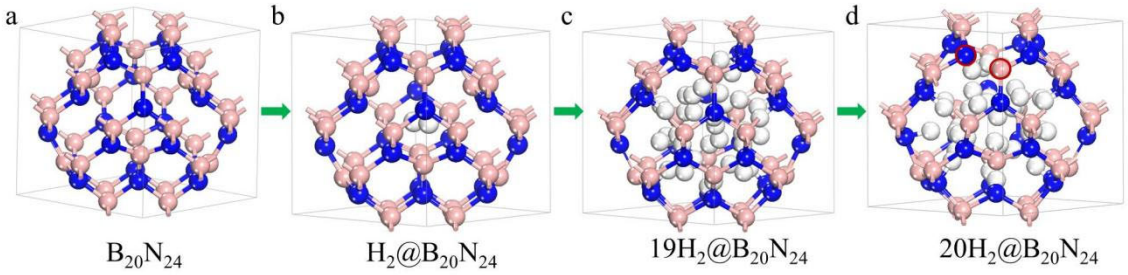

Figure 6. Configurations of the $nH_2@B_{20}N_{24}$ complex as more and more H_2 molecules are stored. The pink, blue and white balls stand for B, N and H atoms, respectively: (**a**) $B_{20}N_{24}$; (**b**) $H_2@B_{20}N_{24}$; (**c**) $19H_2@B_{20}N_{24}$; (**d**) $20H_2@B_{20}N_{24}$.

As we have mentioned above, owing to the high chemical stability of the B–N compounds, this type is a good candidate for hydrogen storage. And, owing to the cage-like configuration of $B_{20}N_{24}$ structure, its storage ability is excellent. As we know, B–N materials are synthesized compounds. These materials are widely used in industries; most of the B–N compounds are semiconductors with wide band gap, and thus, they are also used in electronics. In recent years, more and more B–N materials have been predicted with the help of computational materials science. The studies of the novel structure of this class not only widen the crystal structure information relevant to it, but can also reveal more possible physical properties within the theoretical space. For one thing, in terms of

structural configurations, the results in this work provide a useful method for structural prediction, not only in B–N compounds, but also in many other classes. For another, we provide a new way to design functional material. For example, the cage-like structure can be a candidate in hydrogen storage, and a fully sp^3-hybridzed carbon or BN structure may be a good candidate among superhard materials.

Notably, we should make clear that the first-principles calculations are based on ambient conditions, in which the results are derived under 0 K and 0 GPa. Therefore, the hydrogen storage ability of $B_{20}N_{24}$ structure in this study is determined at 0 K. Considering the vibrations of atoms, the periodic boundary condition and some other conditions during the calculations at 0 K and 300 K, we supposed that the hydrogen storage capacity of $B_{20}N_{24}$ may not be as high as 6.8 wt.%. The hydrogen storage capacity of these B–N compounds at room temperature or at any other temperature, can be derived via molecular dynamics. Normally, it may be lower than the result at 0 K. Theoretically, determining the actual capacity of $B_{20}N_{24}$ at 300 K would require more calculations to reveal. In this work, the $B_{20}N_{24}$ structure is proposed as a novel compound of the B–N system, and can be viewed as a candidate for hydrogen storage, given its highly chemical inertness and cage-like structure.

4. Conclusions

In this paper, a global structural searching of carbon allotropes has been performed, and some novel allotropes with cage-like structures are selected as templates to construct their B–N counterparts by replacing atoms with B and N atoms alternatively. As a result, $B_{20}N_{24}$ is here proposed as a thermodynamically metastable nonstoichiometric N-rich B–N polymorph at ambient pressure. The mechanical and dynamic $B_{20}N_{24}$ has stabilities confirmed by the Born criteria and phonon spectra, respectively. $B_{20}N_{24}$ displays semiconducting features, with a 0.85 eV direct band gap. On the basis of its structural features, $B_{20}N_{24}$ can be seen as a candidate for hydrogen storage. Results show that 19 H_2 molecules, corresponding to 6.8 wt.%, can be stored in $B_{20}N_{24}$. $B_{20}N_{24}$ enriches the structures of B–N compounds, and its unique properties render it a promising functional material for electronic and hydrogen storage applications.

Author Contributions: J.Z.: Software, Conceptualization, Visualization, Writing—Review and Editing. Z.H.: Software. S.X.: Software. M.X.: Conceptualization, Visualization. D.L.: Writing—Review and Editing. Y.W.: Writing—Review and Editing. X.J.: Software, Writing—Original Draft. All authors have read and agreed to the published version of the manuscript.

Funding: This research was funded by [Scientific Research Project of the Education Department of Hubei Province] grant number [B2022172], [National Natural Science Foundation of China] grant number [52002118], [Independent Innovation Projects of the Hubei Longzhong Laboratory] grant number [2022ZZ-03], and [Science and Technology Project of the Hebei Education Department] grant number [QN2022185].

Data Availability Statement: All the data and results supporting this research paper are already presented within this publication.

Acknowledgments: This work is supported by the Scientific Research Project of Education Department of Hubei Province (No. B2022172), National Natural Science Foundation of China (Grant No. 52002118), Independent Innovation Projects of the Hubei Longzhong Laboratory (2022ZZ-03) and Science and Technology Project of Hebei Education Department (QN2022185).

Conflicts of Interest: The authors declare that they have no known competing financial interests or personal relationships that could appear to influence the work reported in this paper.

References

1. Tian, Y.J.; Xu, B.; Yu, D.L.; Ma, Y.M.; Wang, Y.B.; Jiang, Y.B.; Hu, W.T.; Tang, C.C.; Gao, Y.F.; Luo, K.; et al. Ultrahard nanotwinned cubic boron nitride. *Nature* **2013**, *493*, 385–388. [CrossRef] [PubMed]
2. Oku, T.; Kuno, M.; Kitahara, H.; Narita, I. Formation, atomic structures and properties of boron nitride and carbon nanocage fullerene materials. *Int. J. Inorg. Mater.* **2001**, *3*, 597–612. [CrossRef]

3. Chopra, N.G.; Luyken, R.J.; Cherrey, K.; Crespi, V.H.; Cohen, M.L.; Louie, S.G.; Zettl, A. Boron nitride nanotubes. *Science* **1995**, *269*, 966–967. [CrossRef]
4. Pacilé, D.; Meyer, J.C.; Girit, C.O.; Zettl, A. The two-dimensional phase of boron nitride: Few-atomic-layer sheets and suspended membranes. *Appl. Phys. Lett.* **2008**, *92*, 666. [CrossRef]
5. Corso, M.; Auwärter, W.; Muntwiler, M.; Tamai, A.; Greber, T.; Osterwalder, J. Boron Nitride Nanomesh. *Science* **2004**, *303*, 217–220. [CrossRef] [PubMed]
6. Yin, J.; Li, X.; Zhou, J.; Guo, W. Ultralight Three-Dimensional Boron Nitride Foam with Ultralow Permittivity and Superelasticity. *Nano Lett.* **2013**, *13*, 3232–3236. [CrossRef]
7. Strout, D.L. Structure and stability of boron nitrides: Isomers of $B_{12}N_{12}$. *J. Phys. Chem. A* **2000**, *104*, 3364–3666. [CrossRef]
8. Blase, X.; De Vita, A.; Charlier, J.-C.; Car, R. Frustration Effects and Microscopic Growth Mechanisms for BN Nanotubes. *Phys. Rev. Lett.* **1998**, *80*, 1666–1669. [CrossRef]
9. Seifert, G.; Fowler, P.; Mitchell, D.; Porezag, D.; Frauenheim, T. Boron-nitrogen analogues of the fullerenes: Electronic and structural properties. *Chem. Phys. Lett.* **1997**, *268*, 352–358. [CrossRef]
10. Lee, R.S.; Gavillet, J.; de la Chapelle, M.L.; Loiseau, A.; Cochon, J.-L.; Pigache, D.; Thibault, J.; Willaime, F. Catalyst-free synthesis of boron nitride single-wall nanotubes with a preferred zig-zag configuration. *Phys. Rev. B* **2001**, *64*, 121405. [CrossRef]
11. Alexandre, S.S.; Chacham, H.; Nunes, R.W. Structure and energetics of boron nitride fullerenes: The role of stoichiometry. *Phys. Rev. B* **2001**, *63*, 045402. [CrossRef]
12. Zobelli, A.; Ewels, C.P.; Gloter, A.; Seifert, G.; Stephan, O.; Csillag, S.; Colliex, C. Defective structure of BN nanotubes: From single vacancies to dislocation lines. *Nano Lett.* **2006**, *6*, 1955–1960. [CrossRef] [PubMed]
13. Jin, C.; Lin, F.; Suenaga, K.; Iijima, S. Fabrication of a Freestanding Boron Nitride Single Layer and Its Defect Assignments. *Phys. Rev. Lett.* **2009**, *102*, 195505. [CrossRef]
14. Ma, Z.Y.; Zuo, J.; Tang, C.Z.; Wang, P.; Shi, C.L. Physical properties of a novel phase of boron nitride and its potential applications. *Mater. Chem. Phys.* **2020**, *252*, 123245. [CrossRef]
15. Zhang, X.Y.; Liu, Z.F.; Song, T.L.; Cui, X. Sc-$B_{24}N_{24}$: A new low-density allotrope of BN. *J. Phys. Chem. C* **2022**, *126*, 12836–12844. [CrossRef]
16. He, C.; Sun, L.; Zhang, C.; Peng, X.; Zhang, K.; Zhong, J. Z-BN: A novel superhard boron nitride phase. *Phys. Chem. Chem. Phys.* **2012**, *14*, 10967–10971. [CrossRef]
17. Huang, Q.; Yu, D.; Zhao, Z.; Fu, S.; Xiong, M.; Wang, Q.; Gao, Y.; Luo, K.; He, J.; Tian, Y. First-principles study of O-BN: A sp3-bonding boron nitride allotrope. *J. Appl. Phys.* **2012**, *112*, 73-R. [CrossRef]
18. Dai, J.; Wu, X.; Yang, J.; Zeng, X.C. Unusual Metallic Microporous Boron Nitride Networks. *J. Phys. Chem. Lett.* **2013**, *4*, 3484–3488. [CrossRef]
19. Germaneau, E.; Su, G.; Zheng, Q.R. New boron nitride structures B4N4: A first-principles random searching application. *J. Phys. Condens. Matter Inst. Phys. J.* **2013**, *25*, 125504. [CrossRef]
20. Jiang, X.; Zhao, J.; Ahuja, R. A novel superhard BN allotrope under cold compression of h-BN. *J. Physics: Condens. Matter* **2013**, *25*, 122204. [CrossRef]
21. Zhang, S.; Wang, Q.; Kawazoe, Y.; Jena, P. Three-Dimensional Metallic Boron Nitride. *J. Am. Chem. Soc.* **2013**, *135*, 18216–18221. [CrossRef] [PubMed]
22. Dai, J.; Wu, X.; Yang, J.; Zeng, X.C. Porous Boron Nitride with Tunable Pore Size. *J. Phys. Chem. Lett.* **2014**, *5*, 393–398. [CrossRef] [PubMed]
23. Niu, C.-Y.; Wang, J.-T. Three-dimensional three-connected tetragonal BN: Ab initio calculations. *Phys. Lett. A* **2014**, *378*, 2303–2307. [CrossRef]
24. Zhang, Z.; Lu, M.; Zhu, L.; Zhu, L.; Li, Y.; Zhang, M.; Li, Q. Orthorhombic BN: A novel superhard sp3 boron nitride allotrope. *Phys. Lett. A* **2014**, *378*, 741–744. [CrossRef]
25. Wen, B.; Zhao, J.; Melnik, R.; Tian, Y. Body-centered tetragonal B2N2: A novel sp3 bonding boron nitride polymorph. *Phys. Chem. Chem. Phys.* **2011**, *13*, 14565–14570. [CrossRef]
26. Li, Y.; Hao, J.; Liu, H.; Lu, S.; Tse, J.S. High-Energy Density and Superhard Nitrogen-Rich B-N Compounds. *Phys. Rev. Lett.* **2015**, *115*, 105502. [CrossRef] [PubMed]
27. Xie, C.; Ma, M.; Liu, C.; Pan, Y.; Xiong, M.; He, J.; Gao, G.; Yu, D.; Xu, B.; Tian, Y.; et al. Superhard three-dimensional B_3N_4 with two-dimensional metallicity. *J. Mater. Chem. C* **2017**, *5*, 5897–5901. [CrossRef]
28. Lin, S.; Xu, M.; Hao, J.; Wang, X.; Wu, M.; Shi, J.; Cui, W.; Liu, D.; Lei, W.; Li, Y. Prediction of superhard B_2N_3 with two-dimensional metallicity. *J. Mater. Chem. C* **2019**, *7*, 4527–4532. [CrossRef]
29. Ma, R.; Bando, Y.; Zhu, H.W.; Sato, T.; Xu, C.L.; Wu, D.H. Hydrogen uptake in boron nitride nanotubes at room temperature. *J. Am. Chem. Soc.* **2002**, *124*, 7672–7673. [CrossRef]
30. Sun, Q.; Wang, Q.; Jena, P. Storage of Molecular Hydrogen in B−N Cage: Energetics and Thermal Stability. *Nano Lett.* **2005**, *5*, 1273–1277. [CrossRef]
31. Xiao, J.W.; Du, J.L.; Wen, B.; Melnik, R.; Kawazoe, Y.; Zhang, X.Y. Phase stability limit of c-BN under hydrostatic and non-hydrostatic pressure conditions. *J. Chem. Phys.* **2014**, *140*, 164704. [CrossRef] [PubMed]
32. Wentzcovitch, R.; Cohen, M.; Lam, P. Theoretical study of BN, BP, and BAs at high pressures. *Phys. Rev. B* **1987**, *36*, 6058. [CrossRef] [PubMed]

33. Wang, Y.; Jian, L.; Li, Z.; Ma, Y. CALYPSO: A method for crystal structure prediction. *Comput. Phys. Commun.* **2012**, *183*, 2063–2070. [CrossRef]
34. Kresse, G.G.; Furthmüller, J.J. Efficient Iterative Schemes for Ab Initio Total-Energy Calculations Using a Plane-Wave Basis Set. *Phys. Rev. B Condens. Matter* **1996**, *54*, 11169. [CrossRef] [PubMed]
35. Clark, S.J.; Segallii, M.D.; Pickardii, C.J.; Hasnipiii, P.J.; Probertiv, M. First principles methods using CASTEP. *Z. Für Krist. Cryst. Mater.* **2005**, *220*, 567–570. [CrossRef]
36. Ceperley, D.M.; Alder, B.J. Ground State of the Electron Gas by a Stochastic Method. *Phys. Rev. Lett.* **1980**, *45*, 566–569. [CrossRef]
37. Perdew, J.P.; Zunger, A. Self-Interaction Correction to Density-Functional Approximations for Many-Body Systems. *Phys. Rev. B Condens. Matter* **1981**, *23*, 5048–5079. [CrossRef]
38. Heyd, J.; Scuseria, G.E.; Ernzerhof, M. Erratum: "Hybrid functionals based on a screened Coulomb potential" [J. Chem. Phys. 118, 8207 (2003)]. *J. Chem. Phys.* **2006**, *124*, 219906. [CrossRef]
39. Monkhorst, H.J.; Pack, J.D. Special points for Brillouin-zone integrations. *Phys. Rev. B* **1976**, *13*, 5188–5192. [CrossRef]
40. Zhao, Z.; Xu, B.; Zhou, X.-F.; Wang, L.-M.; Wen, B.; He, J.; Liu, Z.; Wang, H.-T.; Tian, Y. Novel Superhard Carbon: C-Centered OrthorhombicC8. *Phys. Rev. Lett.* **2011**, *107*, 215502. [CrossRef]
41. Wu, Z.J.; Zhao, E.J.; Xiang, H.P.; Hao, X.F.; Liu, X.J.; Meng, J. Crystal structures and elastic properties of superhard IrN2 and IrN3 from first principles. *Phys. Rev. B* **2007**, *76*, 054115. [CrossRef]